Atmospheric
Chemistry
and Physics
Open Access
Discussions

Comparison of ice particle characteristics simulated by the Community Atmosphere Model (CAM5) with in-situ observations

T. Eidhammer, H. Morrison, A. Bansemer, A. Gettelman, and A. J. Heymsfield

National Center for Atmospheric Research, P.O. Box 3000, Boulder, CO 80307, USA

Correspondence to: T. Eidhammer (trude@ucar.edu)

ACPD

14, 7637–7681, 2014

Comparison of ice particle characteristics

T. Eidhammer et al.

Title Page

Abstract	Introduction
Conclusions	References
Tables	Figures

|◀ ▶|
◀ ▶
Back Close

Full Screen / Esc

Printer-friendly Version

Interactive Discussion

T. Eidhammer et al.

Abstract

Detailed measurements of ice crystals in cirrus clouds were used to compare with results from the Community Atmospheric Model Version 5 (CAM5) global climate model. The observations are from two different field campaigns with contrasting conditions:
Atmospheric Radiation Measurements Spring Cloud Intensive Operational Period in 2000 (ARM-IOP), which was characterized primarily by midlatitude frontal clouds and cirrus, and Tropical Composition, Cloud and Climate Coupling (TC4), which was dominated by anvil cirrus. Results show that the model typically overestimates the slope parameter of the exponential size distributions of cloud ice and snow, while the variation
with temperature (height) is comparable. The model also overestimates the ice/snow number concentration (0th moment of the size distribution) and underestimates higher moments (2nd through 5th), but compares well with observations for the 1st moment. Overall the model shows better agreement with observations for TC4 than for ARM-IOP in regards to the moments. The mass-weighted terminal fallspeed is lower in the
model compared to observations for both ARM-IOP and TC4, which is partly due to the overestimation of the size distribution slope parameter. Sensitivity tests with modification of the threshold size for cloud ice to snow autoconversion (D_{cs}) do not show noticeable improvement in modeled moments, slope parameter and mass weighed fallspeed compared to observations. Further, there is considerable sensitivity of the cloud
radiative forcing to D_{cs}, consistent with previous studies, but no value of D_{cs} improves modeled cloud radiative forcing compared to measurements. Since the autoconversion of cloud ice to snow using the threshold size D_{cs} has little physical basis, future improvement to combine cloud ice and snow into a single category, eliminating the need for autoconversion, is suggested.

1 Introduction

The parameterization of cloud microphysics plays a critical role in general circulation model (GCM) simulations of climate (e.g., Stephens, 2005). Ice microphysics in particular plays an important role in the global radiative balance (e.g., Mitchell et al., 2008;
5 Zhao et al., 2013), since its parameterization strongly impacts the microphysical and hence radiative properties of ice clouds. It also strongly affects mixed-phase cloud properties, with impacts on precipitation formation and conversion of liquid to ice.

Because traditional GCMs are unable to resolve smaller-scale features that drive cloud processes, and because of the need for computationally efficiency for climate
10 simulations, the parameterization of microphysics in these models has historically been highly simplified. The first GCMs specified cloud properties diagnostically (e.g., see review in Stephens, 2005). In later decades GCMs treated one or more species of cloud water, with precipitation water treated diagnostically (Ghan and Easter, 1992; Rotstayn, 1997; Rasch and Kristjansson, 1998) or prognostically (Fowler et al., 1996;
15 Posselt and Lohmann, 2008). Several earlier schemes partitioned the total condensate into liquid and ice diagnostically as a function of temperature (Del Genio et al., 1996). More recently schemes have begun to separately prognose liquid and ice, with an explicit representation of various processes converting water mass between liquid and ice such as freezing, riming, and the Bergeron–Findeisen–Wegener process (Fowler et al.,
20 1996; Lohmann and Roeckner, 1996; Rotstayn et al., 2000; Morrison and Gettelman, 2008; Gettelman et al., 2010). With the recognition of importance of cloud-aerosol interactions and impacts on droplet and ice crystal sizes and hence radiative properties, additional complexity has been added to GCM microphysics schemes to prognose both mass and number mixing ratios of cloud droplets and ice (Ghan et al., 1997; Lohmann
25 et al., 1999; Liu and Penner, 2005; Ming et al., 2007; Morrison and Gettelman, 2008). Thus, there has been a steady march toward increasing complexity of microphysics schemes in GCMs.

Full Screen / Esc

Nonetheless, several aspects of microphysics remain uncertain. In addition to important issues related to the inability of GCMs to resolve cloud-scale processes, there are underlying uncertainties in the microphysical processes themselves, especially for the ice phase. These uncertainties present challenges, not only for GCMs but also for models of all scales. Much of this uncertainty is rooted in the wide variety of ice particle shapes and types that occur in the atmosphere, leading to a large range of particle fallspeeds, vapor diffusional growth rates, and aggregation efficiencies, to name a few key parameters and processes. Moreover, the parameterization of critical processes like ice nucleation remains uncertain. These uncertainties have important implications for cloud radiative forcing in particular. For example, changes in ice particle fallspeed based on observed ice particle size distributions were found to have a large impact on cirrus coverage and ice water path, with large changes in cloud forcing up to $-5\,\mathrm{W\,m^{-2}}$ in the tropics (Mitchell et al., 2008).

The representation of ice particle properties in most current microphysics schemes is highly simplified. For example, in the Community Atmosphere Model Version 5 (CAM5, Neale et al., 2010), ice particles are represented as spheres (Morrison and Gettelman, 2008). As in nearly all bulk schemes, ice in CAM5 is separated into different categories representing small ice (cloud ice) and larger ice (snow), each with different bulk densities and fallspeed–size relationships. Conversion between cloud ice and snow is parameterized by "autoconversion" that represents the growth of ice particles through vapor diffusion, aggregation, and riming. However, autoconversion has little physical basis since it does not correspond with a specific microphysical process and results in discrete transition of particle properties from cloud ice to snow. The conversion of cloud ice to snow is tuned in CAM5 by modifying the size threshold for autoconversion, D_{cs}.

Another issue is that there is often a lack of self-consistency in ice particle properties in schemes. For example, nearly all bulk schemes (not only in GCMs but in finer-scale models as well) have fallspeed–size relationships that are not directly coupled to particle densities or mass–size relationships, leading to unphysical behavior. For example,

increasing particle density can lead to a *decrease* in mass-weighted mean fallspeed because this leads to a smaller mean particle size, while the fallspeed size relationship depends on mean particle size but not density. As pointed out by Mitchell et al. (2011), self-consistency among these relationships is important because of the physical cou-

⁵ pling of these parameters. For example, the effective radius and mass-weighted mean fallspeed are both dependent upon mass-size and projected area–size relationships, so that a change in these relationships should be reflected in both the fallspeed and effective radius (Mitchell et al., 2011).

Aircraft in-situ observations of ice particles provide an opportunity for detailed test-

¹⁰ ing of assumptions concerning ice particle properties in microphysics schemes. While in situ observations are limited in time and space, statistical comparison with model output, especially in terms of relationships among variables, provides some constraint on microphysics schemes. Here we will investigate how well specific ice microphysical parameters are predicted and diagnosed in CAM5 as compared to in situ observations.

¹⁵ While previous work has evaluated ice microphysics in CAM5 using aircraft observations (Zhang et al., 2013), we provide a more detailed comparison including several size distribution moments as well as mass-weighted fallspeed for two different field campaigns. The focus on several parameters is important because these quantities are closely inter-related. We then evaluate results, including cloud radiative forcing, in

²⁰ the context of sensitivity to the autoconversion size threshold D_{cs} – a key tuning parameter for radiative forcing in CAM5. A unique aspect of this study is that we compare several ice microphysical parameters with the same quantities estimated from observations. To our knowledge this has not been done previously for climate models, but is important because it allows us to dig deeper into reasons for biases in key quantities

²⁵ like mass-weighted fallspeed.

The paper is organized as follows. In Sect. 2, the methodology of this study is presented. In Sect. 2.1 the two aircraft campaigns and associated observations that are used in this study are described, while Sect. 2.2 deals with the model setup. The microphysical parameters that are used for model – observation comparison are detailed

in Sect. 2.3. The comparison results are presented in Sect. 3. Here, the results using default CAM5 parameters are first discussed in Sect. 3.1 while a sensitivity study of the ice–snow autoconversion impact on microphysical parameters is included in Sect. 3.2. Section 4 deals with cloud radiative forcing effects from the autoconversion sensitivity study. Finally, in Sect. 5, a summary and conclusions are presented.

2 Methodology

2.1 Aircraft measurements

Aircraft measurements of ice crystal size distributions from two different field campaigns are used here for the comparison with model results. These observations are from the Tropical Composition, Cloud and Climate Coupling (TC4) (Toon et al., 2010) mission in 2007 and the Atmospheric Radiation Measurements (ARM) Spring Cloud Intensive Operational Period (IOP) (e.g. Dong et al., 2002), in 2000 (hereafter called "ARM-IOP").

The TC4 campaign was based in the tropics (Costa Rica and Panama, see Fig. 1) and one of the main science goals of TC4 was to improve knowledge of how anvil cirrus form and evolve (Toon et al., 2010). The mostly convectively-generated cirrus were sampled by the NASA DC8 aircraft and the subfreezing periods had a low cloud temperature of $\sim -60\,°C$. Particle size distributions were acquired with a Droplet Measurement Technologies (DMT) Cloud Imaging Probe (CIP) sizing from about 50–1000 μm and a 2-D DMT Precipitation Imaging Probe (PIP), (200 μm – 1 cm). Averaging was done over 5 s intervals, with a total in-cloud period of about 20 h ($\sim 15\,600$ km). Total condensed water content (TWC, ice plus liquid when present), were measured with a Counterflow Virtual Impactor (CVI) for TWC > $0.01\,\mathrm{g\,m^{-3}}$. Because of the ice shattering issue, we do not use the small particle probe data (< 75 μm) and modify the CIP data to account for ice shattering using particle interarrival times (see Field et al., 2006). Liquid water was detected and its content estimated from a Rosemount Icing

7642

Probe (RICE). Liquid water encounters were infrequent and have been filtered out of the data set. Further, data were filtered to eliminate updrafts and downdrafts above $1\,\mathrm{m\,s^{-1}}$, and data containing round particles larger than one millimeter in diameter, indicating rain or graupel, were also eliminated.

5   The ARM-IOP was based in the mid-latitudes (Oklahoma, USA, see Fig. 1) and measured a variety of cloud types associated with frontal passages, convection, and synoptically-generated cirrus clouds. Particle size distributions were acquired with a 2-D Cloud (2DC) probe sizing from about 50–1000 µm and a 2-D Precipitation (2DP) probe. The data were acquired with the University of North Dakota Citation Aircraft.

10   Processing was done as noted above, with averaging over 5 s intervals. The total in-cloud time was about 7 h (~ 3400 km). TWC measurements were also made with the CVI and liquid water was detected with the RICE probe. All periods of liquid water were removed from the data set, and the same filtering technique mentioned above was used. A complete discussion of these two data sets, probe evaluations, and processing

15   methods are given in Heymsfield et al. (2013).

2.2   Model setup

The global model from the National Center for Atmospheric Research (NCAR) CAM5 is used in this study. The treatment of clouds in global circulation models is typically divided into parameterization of convective clouds and a more detailed micro-

20   physics treatment of stratiform clouds. CAM5 includes aerosol effects and detailed microphysics only for stratiform clouds, which includes detrained mass from convective anvils. The stratiform microphysics scheme is an updated version (v1.5) of the 2-moment cloud microphysical scheme of Morrison and Gettelman (2008) and Gettelman et al. (2010). Cloud liquid and ice mass and number mixing ratios are prognosed,

25   while rain and snow mass and number mixing ratios are diagnosed. Particle size distributions are assumed to follow gamma functions. Aerosols affect both cloud droplet and ice crystal number concentrations. The version here is noted as MG1.5, where the major change to the microphysics over Gettelman et al. (2010) and relevant to this study,

Comparison of ice particle characteristics

T. Eidhammer et al.

is an improvement in how nucleation of ice is applied to increase crystal number: this is now done consistently with the addition of mass from nucleation before microphysical processes are calculated within the time step.

For this study, we ran CAM5 for six years (from 2000 trough 2005), using the first year as spin up time and analyzing the last five years. We used the Atmosphere Model Intercomparison Program (AMIP) style configuration, with prescribed sea surface temperature (annual cycle of the sea surface temperature which repeats every year) and fixed CO_2 concentrations. The resolution was $1.9° \times 2.5°$, with 30 vertical layers, and global results were output as monthly means. However, over the model grid boxes that overlap the regions from where observations were gathered (Fig. 1), we output instantaneous microphysical parameters and state variables every 3 h. Note that the grid boxes over the TC4 area are chosen such that they cover mainly the ocean due to differences in tuning of the convective microphysics over ocean and land, which can affect radiation and detrained condensate mass feeding into the cloud microphysics.

2.3 Microphysical parameter description

The in situ measurements give detailed information about the size distributions, masses, and projected areas of ice particles, from which mass-weighted terminal fallspeeds can be estimated. The mass-weighted terminal fallspeed is an important factor in controlling lifetime of clouds, as well as controlling many other cloud parameters, since this quantity is relevant for transporting ice and snow mass. It is therefore desirable to match the modeled quantity for mass-weighted terminal fallspeed with observations. For comparing the model and measurements, we will introduce a description of the size distribution parameters used here, and then the calculation of mass-weighted terminal fallspeeds from the model results is described.

Comparison of ice particle characteristics

T. Eidhammer et al.

Title Page

Abstract	Introduction
Conclusions	References
Tables	Figures

|◄ ►|

◄ ►

Back Close

Full Screen / Esc

Printer-friendly Version

Interactive Discussion

2.3.1 Size distribution parameters

First we note that in CAM5, several output microphysical parameters are given as grid-box means rather than in-cloud values. The grid-box mean takes into account of the fraction of the grid-box that contains condensate (snow and cloud ice). Here, all parameters and equations described are for in-cloud values, unless otherwise stated. In MG1.5 (as in nearly all bulk microphysics schemes), snow and cloud ice are divided into two separate categories, with both size distributions (ϕ) assumed to be represented by the gamma functions:

$$\phi(D) = N_0 D^\mu e^{-\lambda D},$$ (1)

where D is the particle diameter, N_0 is the intercept parameter, μ is the shape parameter and λ is the slope parameter. Currently, the shape parameter is set to zero for both snow and cloud ice, meaning that the distributions are represented by inverse exponential functions.

We focus the comparison of modeled and observed size distribution parameters on λ and various size distribution moments (M). Herein we aim on the analysis of the 0th to 5th moments. While mass and number concentrations are proportional to the 0th and 3rd moments, other relevant parameters such as bulk projected area (relevant for collection of cloud water) and mass-weighted fallspeed depend on other moments. Thus, we investigate a range of moments for comparison with observations. The kth moment of the size distribution (M_k), where k is 0 or any positive real number, is found by integrating the distribution in this form:

$$M_k = \int_0^\infty N_0 D^k e^{-\lambda D} dD = \frac{N_0 \Gamma(k+1)}{\lambda^{k+1}},$$ (2)

where Γ is the Euler gamma function. Thus the 0th moment, which is equal to the number concentration (N), can be expressed as

$$M_0 = \frac{N_0}{\lambda} = N. \tag{3}$$

Snow and cloud ice particles are assumed to be spherical in the model, thus the mass concentration, q, is proportional to the 3rd moment:

$$q = \frac{\pi \rho_\mathrm{p}}{6} M_3 = \frac{\pi \rho_\mathrm{p}}{6} \frac{N_0 \Gamma(4)}{\lambda^4} = \frac{\pi \rho_\mathrm{p} N_0}{\lambda^4} = \frac{\pi \rho N}{\lambda^3}. \tag{4}$$

where Eq. (3) is used to relate N_0 to N. Here, ρ_p is the bulk density of the particles. Note, however, that in situ measurements indicate that the mass actually is closer to the 2nd moment than the 3rd since the particles are in reality not spherical. An expression for λ can be found by rearranging terms in Eq. (4):

$$\lambda = \left(\frac{\pi \rho_\mathrm{p} N}{q} \right)^{1/3}. \tag{5}$$

In terms of the moments, λ is proportional to $(M_0/M_3)^{1/3}$.

In CAM5, the λ used by the microphysical process calculations and output from the model is determined before all loss terms for mass and number concentrations are calculated in MG1.5. As a result there is an inconsistency between λ and the mass and number concentrations output by the model. We therefore calculate λ and N_0 offline from the output q and N following Eqs. (3) and (5) to ensure consistency.

A key point is that even though cloud ice and snow are divided into separate categories in MG1.5, the size distributions for each extend from sizes of zero to infinity (i.e., a complete distribution), as in nearly all bulk microphysics schemes. Thus, we must combine the cloud ice and snow distributions to derive parameters for comparing with

Title Page

Abstract | Introduction

Conclusions | References

Tables | Figures

|◀ | ▶|

◀ | ▶

Back | Close

Full Screen / Esc

Printer-friendly Version

Interactive Discussion

observations, which do not differentiate between cloud ice and snow. For λ, this is done by using $N_{si} = N_s + N_i$ and $q_{si} = q_s + q_i$ in Eq. (5), where the subscripts i and s stands for snow and cloud ice, respectively. For ρ_p, we use a mass-weighted density ($\rho_{p,si}$) that combines the snow ($\rho_{p,s}$) and cloud ice ($\rho_{p,i}$) particle densities, specified as 250 and 500 $kg\,m^{-3}$, respectively. However, there is an additional complication when calculating mass-weighted quantities because cloud ice and snow may cover different fractions of the model grid-box. We therefore also take into account the grid-box snow and cloud ice fractions when mass-weighting the density. Note that in MG1.5, the fraction of snow (F_s) is always equal or greater than the fraction of cloud ice (F_i) because it is assumed that the cloud ice is a source of snow, while snow can also fall into non-cloudy parts of the grid-box from above (i.e., the maximum overlap assumption). The mass-weighted snow/ice particle density is therefore given by:

$$\rho_{p,si} = \frac{F_i \frac{\rho_{p,i}q_i + \rho_{p,s}q_s}{q_i + q_s} + (F_s - F_i)\rho_{p,s}}{F_s}, \tag{6}$$

where the left term in the numerator represents the part of the grid-box that contains cloud ice and snow, while the right term represent the part that only contains snow. The entire expression is then weighed by the fraction of the grid-box that snow and cloud ice covers (which, as stated above is equal to the snow fraction).

The λ derived from observations were calculated by linear fit in log-linear space to the measured size distributions. The fits were performed using a principal component analysis to minimize the error normal to the fit line. Only size spectra that provided at least 5 size bins with non-zero concentration were considered in order to maintain a reasonable fit. This threshold was generally met in this study when a measurable size distribution existed from 75 µm to at least 275 µm in diameter. When larger particles were present up to 30 bins were included in the fits. The potential fitting errors, and resulting λ error, depend on the number of bins used for the fit, the number of particles measured in each size bin, and the accuracy of the instruments in a particular size range. These conditions are most favorable in broad size distributions with low λ. Due to

Title Page

Abstract | Introduction

Conclusions | References

Tables | Figures

|◄ | ►|

◄ | ►

Back | Close

Full Screen / Esc

Printer-friendly Version

Interactive Discussion

probe inaccuracies (Strapp et al., 2001) and smaller sample volume for small particles, the errors will be larger for high λ.

For determining the moments in Eq. (2), the integration over D is from zero to infinity. However, the minimum size of ice crystals considered from the observations is 75 μm. Therefore, for consistency the integration of the modeled moments must be done from 75 μm to infinity to directly compare with the measurements:

$$M_k = \int_{D_{min}}^{\infty} N_0 D^k e^{-\lambda D} \mathrm{d}D = \frac{N_0 \Gamma(k+1) \Gamma(k+1, D_{min})}{\lambda^{k+1}}. \tag{7}$$

Here, $\Gamma(k+1, D_{min})$ is the incomplete gamma function. Note that we still use the q and N consistent with integration across the entire size distribution from zero to infinity instead of from D_{min} to infinity to calculate λ using Eq. (5). This is consistent with the λ derived from observations, which were calculated by linear fit in log-linear space to the measured size distributions.

2.3.2 Mass weighted terminal fallspeed

The mass-weighted terminal fallspeed is another parameter derived from observations that we will compare with model results. In CAM5, the size dependent terminal fall-speed (V) is expressed as a power law relation:

$$V = aD^b, \tag{8}$$

where a and b are empirical constants. In MG1.5, a and b have different values for ice and snow ($a_i = 700\,\mathrm{m}^{1-b}\,\mathrm{s}^{-1}$, $b_i = 1$ following Ikawa and Saito (1991) and $a_s = 11.72\,\mathrm{m}^{1-b}\,\mathrm{s}^{-1}$, $b_s = 0.41$ following Locatelli and Hobbs, 1974). For the comparison, we use the mass-weighted terminal fallspeed (V_m), which is obtained by integrating the size distribution (Eq. 1) and weighting by the mass mixing ratio. The mass-weighted

terminal fallspeed can be expressed as:

$$V_{m} = \frac{\int_{D_{min}}^{\infty} \left(\frac{\rho_{a0}}{\rho_a}\right)^{\kappa} \frac{\pi \rho_p}{6} a D^{b+3} \phi(D) dD}{\int_{D_{min}}^{\infty} \frac{\pi \rho_p}{6} D^3 \phi(D) dD} = \frac{\left(\frac{\rho_{a0}}{\rho_a}\right)^{\kappa} \frac{a \Gamma(b+4) \Gamma(b+4, D_{min})}{\lambda^{b+4}}}{\frac{\Gamma(4) \Gamma(4, D_{min})}{\lambda^4}}$$

$$= \left(\frac{\rho_{a0}}{\rho_a}\right)^{\kappa} \frac{a \Gamma(b+4) \Gamma(b+4, D_{min})}{6 \lambda^b \Gamma x(4, D_{min})}. \tag{9}$$

Here, ρ_a is the air density, and ρ_{a0} is typical air density at 850 mb, which is an air density factor based on Heymsfield et al. (2007). For ice, $\kappa = 0.35$ (Ikawa and Saito, 1991) and for snow, $\kappa = 0.54$ (Heymsfield et al., 2007). Relating V_m to the size distribution moments, for cloud ice, V_m is proportional to M_4/M_3 while for snow V_m is proportional to $M_{3.41}/M_3$.

Since the snow and cloud ice categories are not distinguished in the observations, the modeled snow and cloud ice V_m need to be combined into $V_{m,si}$ in order to compare with observations. We follow the same formulation as for the mass-weighted particle density:

$$V_{m,si} = \frac{F_i \frac{V_{m,i} q_i + V_{m,s} q_s}{q_i + q_s} + (F_s - F_i) V_{m,s}}{F_s}, \tag{10}$$

where $V_{m,s}$ and $V_{m,i}$ are the snow and cloud ice mass-weighed terminal fallspeed respectively.

In regards to measurements, the mass-weighted fallspeeds from the in-situ observations were computed from the technique (and coefficients) described in Heymsfield and Westbrook (2010). They included the area ratio of the particles (area of the particle's projected area to the area of a circumscribing disk) when determining the mass-weighted fallspeeds.

2.3.3 Critical diameter for ice snow autoconversion

In MG1.5, the conversion of cloud ice to snow via "autoconversion" is treated by transferring mass and number mixing ratio from condensate (ice) to precipitation (snow) based on the critical size threshold, D_{cs} and an assumed conversion timescale (Morrison and Gettelman, 2008). Expressions for the grid-scale tendencies are:

$$\left(\frac{\partial q_i'}{\partial t}\right)_{auto} = -F_i\frac{\pi\rho_i N_{0i}}{6\tau_{auto}}\left[\frac{D_{cs}^3}{\lambda_i} + \frac{3D_{cs}^2}{\lambda_i^2} + \frac{6D_{cs}}{\lambda_i^3} + \frac{6}{\lambda_i^4}\right]e^{-\lambda_i D_{cs}}$$

$$\left(\frac{\partial N_i'}{\partial t}\right)_{auto} = -F_i\frac{N_{0i}}{\lambda_i \tau_{auto}}e^{-\lambda_i D_{cs}} \tag{11}$$

(Morrison and Gettelman, 2008). Here $\tau_{auto} = 3\,\text{min}$ is the assumed autoconversion time scale. The quantities with a prime denote the grid-box average values. Since cloud ice and snow have much different particle densities and terminal fallspeed parameters (as described in Sects. 2.3.1 and 2.3.2), there is a discontinuity of bulk ice properties after conversion from cloud ice to snow. The parameter D_{cs} is chosen rather arbitrary and is one of the main tuning parameters in CAM5: for a given N_i, a larger value for D_{cs} allows higher cloud ice water content before conversion to snow. The default value for D_{cs} in MG1.5 is 250 μm but we will also show results with $D_{cs} = 80, 100, 150, 400$ and 500 μm in Sect. 3.2, which is similar to the range of D_{cs} tested by Zhao et al. (2013). However, we first describe comparison of the model and observations using the default value of D_{cs} in Sect. 3.1.

Full Screen / Esc

Printer-friendly Version

Interactive Discussion

3   Results

3.1   Control model–observations comparison (D_{cs} = 250 µm)

The measurements were mainly collected in cirrus clouds, but the formation mechanisms generally differed between the TC4 and ARM-IOP cases (Heymsfield et al., 2013). The cirrus in TC4 were mainly anvils associated with deep convection while the cirrus from the ARM-IOP were in situ-generated. We therefore expect to see some differences in the modeled parameters between the two locations, as also seen in the observations (Heymsfield et al., 2013). First we compare the slope parameter λ between model and measurements.

3.1.1   Slope parameter

Figure 2 shows the modeled (red) and measured (black) λ as a function of temperature (which is nearly analogous to height). The solid lines are the geometric mean of the measured or modeled λ. The modeled λ is about a factor of 2 higher than the observed across the entire range of temperatures analyzed. As shown below, this difference between the model results and observations results from both an over-prediction of N (M_0) and under-prediction of q (proportional to M_3). However, the change in λ as a function of temperature is fairly similar between model and observations. By fitting the data to the exponential equation $\lambda = Ae^{-BT}$, the B coefficient for modeled and measured fitted data for ARM-IOP are, respectively, −0.028 and −0.025, while for TC4 they are −0.03 and −0.032. Note that in Heymsfield et al. (2013), the B coefficient determined for TC4 is −0.0868. In their paper, the size distribution shape parameter (μ) is not assumed to be zero, as we assume in this study. A non-zero μ results in a steeper λ–T relationship and hence B decreases (becomes more negative). A smaller B coefficient value (−0.0292) is not seen in the ARM-IOP case in the Heymsfield et al. (2013) paper.

The reason that λ decreases with increasing temperature in the model is mainly due to the change in the ratio of snow to cloud ice mass as temperature increases (or as height decreases). Figure 3 shows that when the modeled λ is calculated individually for snow and cloud ice, λ is fairly constant over all temperatures (except for cloud ice at very low temperatures for TC4). The cloud ice category has larger λ values than snow, and larger λ shifts the size distribution to smaller sizes. When considering Figs. 2 and 3, it is clear that cloud ice mass dominates at low temperatures ($< -50\,°C$), while snow mass dominates at relatively higher temperatures ($> -20\,°C$); the combined λ is closer to λ_i at low temperatures and closer to λ_s at warmer temperatures. This is partly explained by the limited amount of vapor available for growing ice particles at lower temperatures. In addition, more ice particles are typically nucleated at low temperatures, and there is more competition for the available vapor. Thus, mean particle size tends to be smaller at low temperatures, and conversion from cloud ice to snow is limited.

3.1.2 Moments

Figures 4 and 5 show the moments for ARM-IOP and TC4, respectively. Recall that the zero moment (M_0) is the same as the number concentration, N_0. For ARM-IOP, M_0 is overestimated by about a factor of 2 between $-35\,°C$ and $-10\,°C$, while at temperatures lower than $-40\,°C$ the model underestimates compared to the measurements. For deposition ice nucleation in CAM5, the parameterization by Meyers et al. (1992) is used at temperatures $> -37\,°C$ (but with constant freezing rate at temperatures $< -20\,°C$). It has been shown in several papers that this parameterization will typically over-predict ice nucleation by at least an order of magnitude (e.g., Prenni et al., 2007; DeMott et al., 2010). Here the differences in number concentration are much smaller and the assumption of holding the freezing rate constant for deposition nucleation at temperatures $< -20\,°C$ seems to improve prediction of ice nucleation at temperatures warmer than $-40\,°C$. At lower temperatures ($< -4\,°C$), the ice nucleation scheme in CAM5 allows for competition between heterogeneous and homogeneous freezing of deliques-

cence aerosols (Liu and Penner, 2005). In this scheme, heterogeneous ice nucleation occurs in the form of immersion freezing of dust, and is based upon classical nucleation theory. In certain cases, for in situ generated cirrus, heterogeneous ice nucleation on a few aerosols will start at lower ice saturation than for homogeneous freezing of deli-
5   quescence aerosols (e.g. DeMott et al., 1997; Gierens, 2003). These newly formed ice crystals can rapidly deplete the vapor by vapor diffusion, limiting homogeneous aerosol freezing and leading to small ice crystal concentration. If, on the other hand, the number of heterogeneous frozen ice crystals is small enough, homogeneous freezing can still occur and the resulting ice crystal concentration can be fairly high (e.g. Barahona
10 and Nenes, 2009; Eidhammer et al., 2009). It is possible that the prediction of ice crystals is too aggressive at lower temperatures, where the classical nucleation theory for immersion freezing is used (e.g. Zhang et al., 2013; Eidhammer et al., 2009). This may be why we see an underestimation of M_0 at temperatures below $-40\,°C$ because the competition between heterogeneous and homogeneous nucleation leads to suppres-
15 sion of homogeneous freezing of deliquescence aerosols. Zhang et al. (2013) came to a similar conclusion in their study with CAM5.

The measurements only go down to $-55\,°C$, thus we cannot say how well the model performs at lower temperatures. For M_0 at temperatures between -10 and $-35\,°C$, both the model and observations show a decrease in M_0 as a function of temperature
20 with a similar rate of change.

The first moment (M_1), which represents the total integrated particle size of the snow and cloud ice population, has similar trends to M_0 for ARM-IOP, with overestimation at higher temperatures ($T > -30\,°C$) and underestimation at lower temperatures. For the higher moments, M_2 shows a reasonable agreement at temperatures between -25
25 and $-10\,°C$, while there is still an underestimation at lower temperatures. For M_3, M_4 and M_5, the model underestimates values over almost the entire temperature regime, while the trend with temperature is in slightly better agreement than for the smaller moments.

When considering the TC4 moments (Fig. 5), the modeled M_0 in general compares better with observations than for ARM-IOP. However, the model still overestimates M_0, with about a factor of 1.5 for temperatures less than −10 °C. The competition between homogeneous and heterogeneous nucleation does not happen readily in convective clouds, thus the underestimation seen in the ARM-IOP at cold temperatures is less likely to occur. Note that although the observations and model results for TC4 considered here are of stratiform cloud types (anvil cirrus), they are detrained by convective clouds. The slope of M_0 with temperature is again similar between the model and observations. The first moment (M_1) shows a remarkably close agreement between observations and model. However, when considering the higher moments (M_2, M_3, M_4 and M_5), the model tends to have lower values compared to observations. Again, the rate of change of the moments with temperature is about the same between the model and observations at temperatures less than −10 °C. Interestingly, both the model and observations show a slight increase in M_4 and M_5 at around −30 °C. Overall, the TC4 model results are in better agreements with observations than for the ARM-IOP case.

Since N is typically higher in the model than in the observations, while q is lower, it is clear that both factors contribute to the positive bias in the modeled slope parameter (λ) seen in Fig. 2, since λ is proportional to $(N/q)^{1/3}$ according to Eq. (5).

3.1.3 Mass weighted terminal fallspeed

Figure 6 shows the mass-weighted terminal fallspeeds (V_m). Figure 6a compares V_m from the model and observations for both TC4 and ARM-IOP. Figure 6b (TC4) and c (ARM-IOP) are included to show the spread of V_m for the model and observations. In general, V_m determined from the model are somewhat lower than the V_m derived from measurements. Furthermore, TC4 tends to have higher V_m than ARM-IOP, and this is seen in both the model and observations. The V_m at temperatures above −25 °C (−20 °C) increase sharply in the TC4 (ARM-IOP) observations, while the modeled V_m show less variation with temperature in this region. However, note that there are very few measurements at temperatures above about −20 °C for ARM-IOP and TC4. At

Title Page

Abstract | Introduction

Conclusions | References

Tables | Figures

|◄ | ►|

◄ | ►

Back | Close

Full Screen / Esc

Printer-friendly Version

Interactive Discussion

lower temperatures ($< -25\,°C$), the V_m derived from observations are about a factor of 1.2 higher in the TC4 case compared to the model, but the trend of modeled V_m with temperature is in reasonable agreement with observations. There is less variation of V_m with temperature for the ARM-IOP observations compared to TC4, which is not captured by the model. The increase of V_m with temperature in the model mostly reflects an increase in the ratio of snow to cloud ice, since V_m is inversely proportional to λ while λ does not vary much with temperature for cloud ice and snow individually (see Fig. 3). Thus, the trend of V_m with temperature in the model is mostly controlled by conversion of cloud ice to snow, which influences the mass densities and fallspeeds. As described in Sect. 4, this conversion has a limited physical basis. Further, the physical reason for the general increase of V_m with temperature in the model is the increase of mean particle size (combined cloud ice and snow) with temperature, consistent with the change in λ with temperature (see Fig. 2). As can be seen in the model, V_m at temperatures less than $-60\,°C$ is smaller than $0.3\,\mathrm{m\,s^{-1}}$ and small ice is dominating in this region.

In general, smaller modeled V_m compared to observations is expected since V_m is inversely proportional to λ (see Eq. 9). Since the modeled λ is larger than measured (see Fig. 2), the modeled V_m should be smaller than those derived from measurements. To illustrate the effect that the factor of 2 in bias for λ has on V_m, we calculated V_m, assuming snow and cloud ice $\lambda = \lambda/2$ (Fig. 7, blue curves). Where snow dominates the total ice mass results are now closer to observations, but where cloud ice is prevalent the V_m are still lower in the model than the observations.

The modeled V_m are not only dependent on λ, but also on the assumed power law fallspeed-size parameters for cloud ice and snow in Eq. (8). To test the sensitivity to these parameters, we ran a simulation with a_i and a_s increased by 50 %. These results are also shown in Fig. 7 (green curves). At lower temperatures, where cloud ice dominates the total ice mass, V_m does not change much. However, at higher temperatures where snow contributes more significantly to the total mass, V_m increases by about 50 %. This is seen in both the ARM-IOP and TC4 cases. For the ARM-IOP case,

Title Page

Abstract | Introduction

Conclusions | References

Tables | Figures

|◄ | ►|

◄ | ►

Back | Close

Full Screen / Esc

Printer-friendly Version

Interactive Discussion

the increase in *a* is clearly too large compared to observations, but for the TC4 case, the comparison between model and observations improves (but still has values somewhat larger than those from observations). This may reflect differences in fallspeed parameters between in situ and anvil cirrus as suggested by observations (Heymsfield et al., 2013). However, the increased *a* parameter in the simulations probably compensates for the over-prediction of λ. Thus, this result does not suggest that *a* should be increased by up to 50 % to obtain better agreement with observations. Rather, it suggests the importance of accurately predicting λ as well as specifying realistic values of the fallspeed parameters.

3.2 Cloud ice to snow autoconversion sensitivity tests

As shown in Sect. 3.1, the model does a reasonable job in predicting some of the size distribution parameters and aspects of the mass-weighted terminal fallspeed. However, there are still clear discrepancies between model results and observations. Moreover, the trends of λ, V_{m}, and the size distribution moments with temperature in the model are mainly controlled by the partitioning of cloud ice and snow, which is primarily determined by cloud ice to snow autoconversion but has limited physical basis as described below. The critical size for autoconversion of cloud ice to snow, D_{cs}, is one of the major tuning parameters in CAM5. For example, Zhao et al. (2013) found that among 16 parameters in CAM5, the top of atmosphere radiative forcing responded most efficiently to the tuning of D_{cs} (changes in cloud ice and snow fallspeed parameters and the lower limit on cloud droplet number had smaller impact). When cloud ice is converted to snow, mass and number mixing ratios are moved from one category to another, with discrete changes to particle density and the fallspeed parameters. Cloud ice to snow autoconversion has a limited physical basis since it does not represent a specific microphysical process, and hence the "best" value for D_{cs} is not well established empirically or theoretically. If it is tuned to make the model results comparable with observed cloud radiative forcing, the calculation of other important microphysical parameters might be degraded (Zhang et al., 2013). For example, Zhang et al. (2013) found

that using $D_{cs} = 250\,\mu m$ led to close agreement with observations from the SPARTI-CUS (Small Particles in Cirrus) campaign for the effective particle size, while the total cloud radiative forcing (shortwave + longwave) at the top of the atmosphere was closer to observations when using higher D_{cs} values. However, as shown in Sect. 3.1, sev-5 eral microphysical parameters that we compared showed rather poor agreement using $D_{cs} = 250\,\mu m$. Here we compare the same parameters as above, but across a range of settings for D_{cs}.

We conducted 5 additional simulations with $D_{cs} = 80$, 100, 150, 400 and 500 µm. We chose a rather wide span of D_{cs} settings since this parameter is not constrained 10 physically. The range of values tested here is similar to Zhao et al. (2013) (100–500 µm) and larger than in Zhang et al. (2013) (175–325 µm) and Gettelman et al. (2010) (150–250 µm). Figure 8 shows λ for all the different D_{cs} values. Overall, none of the values of D_{cs} tested improves the comparison with observation, and hence λ is still too large in the model. The differences between the various runs are not monotonic with changes 15 in D_{cs} and do not show a clear trend with temperature (at some temperatures they are higher than the control run, at some temperatures they are lower, regardless if D_{cs} is higher or lower than in the control run).

Figures 9 and 10 show the moments for ARM-IOP and TC4, respectively. For the number concentration (M_0) in the ARM-IOP case there is a clear increase with smaller 20 D_{cs} values. When D_{cs} is increased, there is only a change in M_0 at the highest tem-peratures (above −20 °C). None of the various D_{cs} simulations significantly improve M_0 compared to measurements. For M_1, the higher values of D_{cs} improve the comparison slightly at temperatures above about −30 °C. For larger moments the simulations are similar at higher temperatures, but there are some differences at lower temperatures. 25 $D_{cs} = 80\,\mu m$ compares slightly better at low temperatures for M_1, M_2 and M_3, but over-all, the moment comparison with observations does not notably improve by varying D_{cs} for the ARM-IOP case.

When considering the moments for TC4, the trend of number concentration, M_0, with temperature shows a slightly different picture than in the ARM-IOP case. Simula-

Title Page

Abstract | Introduction

Conclusions | References

Tables | Figures

◄ | ►

◄ | ►

Back | Close

Full Screen / Esc

Printer-friendly Version

Interactive Discussion

tions with large D_{cs} produce the largest M_0 at low temperatures. However, this trend reverses at higher temperatures, so that simulations with small D_{cs} have the largest M_0. Nonetheless, the trend in M_0 with temperature still compares best with measurements when using $D_{cs} = 250\,\mu m$. For M_1, the $D_{cs} = 250\,\mu m$ simulation also compares best with measurements, while for the higher moments, the sensitivity to D_{cs} cases is smaller, with all simulations exhibiting bias compared to observations.

It is clear that changes in D_{cs} have a large impact on the mass-weighted terminal fallspeed V_m (Fig. 11). When cloud ice is converted to snow at relatively small sizes ($D_{cs} = 80\,\mu m$), V_m is almost the same at all temperatures. This is because the particles are mainly snow, and the slope parameter λ for snow is almost constant in this case (see Fig. 3, and note that the $D_{cs} = 80\,\mu m$ case has a similar temperature trend for snow, only with somewhat higher values).

When the conversion from cloud ice to snow occurs at larger sizes ($D_{cs} > 400\,\mu m$), V_m is small at low temperatures, and only increases to larger values at temperatures above about $-50\,°C$. At higher temperatures V_m is largest with $D_{cs} = 500\,\mu m$. This occurs because conversion from cloud ice to snow is delayed when D_{cs} is large, so that the mean particle size and hence V_m are relatively large once cloud ice is converted to snow. The higher D_{cs} simulations have a comparable temperature trend for TC4, but V_m are still too low compared to observations. In summary, none of the values of D_{cs} gives a clearly improved comparison with observations for the parameters analyzed here.

4 Sensitivity of cloud radiative forcing to D_{cs}

In the previous section we showed that changing D_{cs} has a large impact on the mass-weighted terminal fallspeed and the smaller moments in the size distribution. As changes in D_{cs} impact V_m and other processes (such as Bergeron–Findeisen process, i.e. the conversion of liquid to ice through ice depositional growth), the liquid and ice water paths change as well as the effective radii. These changes in turn impact the cloud radiative forcing consistent with previous studies (Gettelman et al., 2010; Zhao et al.,

2013; Zhang et al., 2013). These studies used MG microphysics in CAM5 and showed that, globally, it is the longwave cloud forcing that is most influenced by changes to D_{cs}. Gettelman et al. (2010) and Zhao et al. (2013) also showed that the changes in total cloud forcing (longwave plus shortwave) varies in magnitude as a function of latitude,

5 with the mid-latitudes experiencing the largest changes in terms of sensitivity to D_{cs}. Moreover, as previously stated, Zhang et al. (2013) found that among 16 different parameters, changes to D_{cs} had the largest impact on top of the atmosphere radiation. In our simulations, with regard to changes to D_{cs}, we come to some of the same conclusions. Here we also show which microphysical variables have the most impact on the

10 cloud radiative forcing through changes in D_{cs}.

Figure 12 shows how the zonally-averaged shortwave and longwave radiative cloud forcing (SWCF and LWCF respectively) is affected by changes to D_{cs} as a function of latitude. The LWCF has an increase with increasing D_{cs} over all latitudes, while the SWCF has opposite effects between mid-latitudes and tropics. The cloud radiative forc-

15 ing is dependent upon the ice and snow effective radii (proportional to M_3/M_2) as well as ice and snow water contents (proportional to M_3), in addition to cloud droplet effective radius and cloud liquid water content. To investigate which quantities are the major controlling factors in the sensitivity of cloud radiative forcing to D_{cs}, we plot several key zonally-averaged quantities in Fig. 13. Figure 13a–d shows the combined cloud ice

20 plus snow water path, cloud liquid water path, snow water path and cloud ice water path, respectively (note that the water path is the vertical integral of the water content). Figure 13e shows the effective radii of cloud ice and snow, while Fig. 13f shows the effective radius of cloud droplets.

As D_{cs} increases, less cloud ice is converted to the snow category, as is shown

25 monotonically in Fig. 13c and d at mid-latitudes. There is limited impact on the total cloud ice plus snow water path in the mid latitudes since changes in the snow and cloud ice water paths have opposing effects (Fig. 13a). In the tropics, on the other hand, there is some increase in the combined snow and cloud ice water path, since there is a slight increase in snow water path relative to the decrease in ice water path

with increasing D_{cs} (see Fig. 13c). If TC4 is representative of the zonally-averaged snow water path in the tropics, based on the analysis presented in Sect. 3, we suspect that the higher snow water path with larger D_{cs} is due to increases in snow at relatively high temperatures, i.e., lower altitudes (not shown). However, it is clear from all the parameters shown in Fig. 13 that the change in cloud ice water path is one of the main controlling factor in the changes to LWCF (Fig. 12b). For example, details such as the clustering of cloud ice water path for the simulations with D_{cs} less than 250 μm are closely mirrored in LWCF.

SWCF is also a function of liquid, snow and cloud ice water paths and effective radii. Figure 12a shows that the response of SWCF to changes in D_{cs} has opposite effects in mid-latitudes compared to the tropics. By comparing Fig. 12a with Fig. 13, it is clear that the cloud liquid water path is the primary controlling factor in explaining the SWCF changes. Snow water path has some of the same variations as cloud liquid water path with D_{cs} (higher water path in tropics with increasing D_{cs} and lower in the mid-latitudes). However, overall changes in the cloud liquid water path with D_{cs} mirror changes in SWCF closer than changes in snow water path. Thus, the shortwave cloud forcing response appears to be mostly explained by indirect impacts of D_{cs} on liquid water path rather than directly through changes in the cloud ice and snow radiative properties. Furthermore, there is little correspondence between changes in the effective radii of snow, cloud ice, or liquid and SWCF with modification of D_{cs}. This is seen in Figs. 12 and 13, which show little correspondence between changes in effective radii and SWCF, compared to changes in liquid water path.

Finally, we show the zonally-averaged total cloud radiative forcing (TCF, SWCF + LWCF) in Fig. 14. Overall, the magnitude of TCF decreases with increasing D_{cs}, moving the modeled TCF closer to CERES observations. However, the magnitude of the modeled TCF is still over-estimated compared to the observations in the tropics and into the mid-latitudes. Only in a small window in the Southern Hemisphere (−60 to −70°) do D_{cs} cases ≤ 250 μm compare well with the observations. In summary, variations in D_{cs} impose a relatively large change in cloud radiative forcing, but none of the

Comparison of ice particle characteristics

T. Eidhammer et al.

Title Page

Abstract | Introduction

Conclusions | References

Tables | Figures

|◄ | ►|

◄ | ►

Back | Close

Full Screen / Esc

Printer-friendly Version

Interactive Discussion

values tested here notably improve the modeled cloud radiative forcing compared to observations.

5   Summary and conclusions

We have presented a global circulation model – observational comparison of important microphysical parameters, such as the size distribution slope parameter, moments of the snow and ice particle size distributions, and mass-weighted fallspeed. These parameters are closely linked to the direct radiative forcing of cloud ice and snow, and also have important indirect effects by impacting cloud liquid. It is therefore crucial to obtain a good agreement between model and observations of snow and ice size distributions parameters in the model, in order to conduct climate impact studies.

We used CAM5 with the MG1.5 microphysics for this study. The aircraft observations were collected during TC4 (tropical anvil cirrus) and ARM-IOP (mid-latitude continental in-situ generated cirrus).

Our results with the control simulation (D_{cs} = 250 µm) indicate that the slope parameter in MG1.5 is about a factor of two higher than that determined with observations. This is true for both regions. However, the trend with temperature is comparable. For the moments, the model generates about a factor of two larger ice crystal number concentrations (ice plus snow) at relatively high temperatures, while the ARM-IOP case indicate that the model generates too few crystals at low temperatures. We hypothesize this results from too many ice crystals formed heterogeneously at temperatures < −37 °C, so that the competition between homogeneous and heterogeneous nucleation does not allow for homogeneously formed ice crystals and thus we see a higher crystal concentration. This is consistent with Zhang et al. (2013), who used SPARTICUS data in their evaluation of ice nucleation schemes in CAM5. The first moment has the best comparison between model and observations, while higher moments are generally underpredicted (including the 3rd moment, proportional to ice water content in the model).

The mass-weighted fallspeeds were about a factor of 1.2 lower in the model compared to observations.

In MG1.5, as in nearly all bulk microphysics schemes, ice is separated into cloud ice and snow categories with different particle densities and fallspeed parameters. The size threshold for conversion of cloud ice to snow, D_{cs}, is one of the main tuning parameters for cloud radiative forcing in CAM5. We conducted five additional simulations covering a large range of D_{cs} values. However, none of these simulations notably improved the comparison between the model and observations of the size distribution parameters and mass-weighted fallspeed. We note that the snow is determined diagnostically in MG1.5 and therefore is assumed to be in steady state within a time step (i.e. the source and sink terms are equal to what is removed due to fallout). In this case, snow still undergoes processes such as sublimation, melting and riming. However, if snow was determined prognostically the steady state assumption no longer applies and there is memory of snow mass and number mixing ratios across time steps (work is underway to modify CAM5 microphysics to include prognostic rain and snow). Thus, there could be differences in the sensitivity to D_{cs} in a prognostic snow scheme compared to the diagnostic snow scheme examined here.

The changes to D_{cs} also have large impacts on cloud radiative forcing. Changes in the total ice water path (cloud ice plus snow) with D_{cs} were fairly small, especially in mid-latitudes, because of opposing effects on the cloud ice and snow water paths. However, the longwave cloud radiative forcing is primarily influenced by cloud ice water path and hence the increase in cloud ice water path with increasing D_{cs} led to an increase in longwave cloud forcing. On the other hand, changes in the shortwave cloud forcing were mostly influenced by changes in cloud liquid water path indirectly driven by changes in D_{cs}. Overall, there was a noticeable change in total cloud forcing when increasing D_{cs} from 250 μm, especially in the mid-latitudes. For example, there was a 10 Wm^{-2} increase in total cloud radiative forcing in the southern mid-latitudes when D_{cs} was increased from 250 μm to 400 μm. The changes were somewhat smaller in

Comparison of ice particle characteristics

T. Eidhammer et al.

Large sensitivity of the size distribution parameters and moments and mass-weighted fallspeed, as well as cloud radiative forcing, to D_{cs} motivates additional work to improve how ice particle properties change with increasing particle size. This is especially true given that no particular value of D_{cs} led to substantially better overall results. Furthermore, the autoconversion of cloud ice to snow, using the threshold size D_{cs}, has little physical basis. One possible approach is to combine cloud ice and snow into a single category such as proposed by Morrison and Grabowski (2008), entirely removing the need for autoconversion. Ice particle mass-size and projected area–size relationships (from which fallspeed–size relationship would be derived) would then vary across the particle size distribution to represent the different properties of small and large ice particles specified from observations. This would lead to some complication because simple analytic integrations, for example for the mass-weighted fallspeed, are no longer possible. However, numerical integration can be performed with values stored in a lookup table (as used by Morrison and Grabowski, 2008), or with simplified expressions based on curve-fitting. Future work will explore these ideas.

References

Barahona, D. and Nenes, A.: Parameterizing the competition between homogeneous and heterogeneous freezing in cirrus cloud formation – monodisperse ice nuclei, Atmos. Chem. Phys., 9, 369–381, doi:10.5194/acp-9-369-2009, 2009.

Del Genio, A. D., Yao, M.-S., Kovari, W., and Lo, K. K.-W.: A prognostic cloud water parameterization for climate models, J. Climate, 9, 270–304, 1996.

DeMott, P. J., Rogers, D. C., and Kreidenweis, S. M.: The susceptibility of ice formation in upper tropospheric clouds to insoluble aerosol components, J. Geophys. Res., 102, 19575–19584, doi:10.1029/97JD01138, 1997.

DeMott, P. J., Prenni, A. J., Liu, X., Kreidenweis, S. M., Petters, M. D., Twohy, C. H., Richardson, M. S., Eidhammer, T., and Rogers, D. C.: Predicting global atmospheric ice nuclei distributions and their impacts on climate, P. Natl. Acad. Sci. USA, 107, 11217–11222, 2010.

Dong, X., Mace, G. G., Minnis, P., Smith, W. L., Poellot, M., Marchand, R. T., and Rapp, A. D.: Comparison of stratus cloud properties deduced from surface, GOES, and aircraft data during the March 2000 ARM Cloud IOP, J. Atmos. Sci., 59, 3265–3284, 2002.

Eidhammer, T., DeMott, P. J., and Kreidenweis, S. M.: A comparison of heterogeneous ice nucleation parameteriza- tions using a parcel model framework, J. Geophys. Res., 114, D06202, doi:10.1029/2008JD011095, 2009.

Field, P. R., Heymsfield, A. J., and Bansemer, A.: Shattering and particle interarrival times measured by optical array probes in ice clouds, J. Atmos. Ocean. Tech., 23, 1357–1371, doi:10.1175/JTECH1922.1, 2006

Fowler, L. D., Randall, D. A., and Rutledge, S. A.: Liquid and ice cloud microphysics in the CSU General Circulation Model. Part I: Model description and simulated microphysical processes, J. Climate, 9, 489–529, 1996.

Gettelman, A., Liu, X., Ghan, S. J., Morrison, H., Park, S., Conley, A. J., Klein, S. A., Boyle, J., Mitchell, D. L., and Li, J.-L. F.: Global simulations of ice nucleation and ice supersaturation with an improved cloud scheme in the Community Atmosphere Model, J. Geophys. Res., 115, D18216, doi:10.1029/2009JD013797, 2010.

Ghan, S. J. and Easter, R. C.: Computationally efficient approximations to stratiform cloud microphysics parameterization, Mon. Weather Rev., 120, 1572–1582, 1992.

Ghan, S. J., Leung, L. R., and Easter, R. C.: Prediction of cloud droplet number in a general circulation model, J. Geophys. Res., 102, 21777–21794, 1997.

Gierens, K.: On the transition between heterogeneous and homogeneous freezing, Atmos. Chem. Phys., 3, 437–446, doi:10.5194/acp-3-437-2003, 2003.

Heymsfield, A. J. and Westbrook, C. D.: Advances in the estimation of ice particle fall speeds using laboratory and field measurements, J. Atmos. Sci., 67, 2469–2482, 2010.

Heymsfield, A. J., Bansemer, A., and Twohy, C. H.: Refinements to ice particle mass dimensional and terminal velocity relationships for ice clouds. Part I: Temperature dependence, J. Atmos. Sci., 64, 1047–1067, 2007.

Comparison of ice particle characteristics

T. Eidhammer et al.

Title Page

Abstract	Introduction
Conclusions	References
Tables	Figures

|◀ | ▶|

◀ | ▶

Back | Close

Full Screen / Esc

Printer-friendly Version

Interactive Discussion

Heymsfield, A. J., Schmitt, C., and Bansemer, A: Ice cloud particle size distributions and pressure-dependent terminal velocities from in situ observations at temperatures from 0° to −86 °C, J. Atmos. Sci., 70, 4123–4154, doi:10.1175/JAS-D-12-0124.1, 2013.

Ikawa, M. and Saito, K.: Description of a non-hydrostatic model developed at the Forecast Research Department of the MRI, MRI Tech. Rep. 28, 238 pp., 1991.

Liu, X. and Penner, J. E.: Ice nucleation parameterization for global modelsm, Meteorol. Z., 14, 499–514, 2005.

Locatelli, J. D. and Hobbs, P. V.: Fall speeds and masses of solid precipitation particles, J. Geophys. Res., 79, 2185–2197, doi:10.1029/JC079i015p02185, 1974.

Lohmann, U. and Roeckner, E.: Design and performance of a new cloud microphysics scheme developed for the ECHAM general circulation model, Clim. Dynam., 12, 557–572, 1996.

Lohmann, U., Feichter, J., Chuang, C. C., and Penner, J. E.: Prediction of the number of cloud droplets in the ECHAM GCM, J. Geophys. Res., 104, 9169–9198, 1999.

Meyers, M. P., Demott, P. J., and Cotton, W. R.: New primary ice nucleation parameterizations in an explicit cloud model, J. Appl. Meteorol., 31, 708–721, 1992.

Ming, Y., Ramaswamy, V., Donner, L. J., Phillips, V. T., Klein, S. A., Ginoux, P. A., and Horowitz, L. W.: Modeling the interactions between aerosols and liquid water clouds with a self-consistent cloud scheme in a general circulation model, J. Atmos. Sci., 64, 1189–1209, 2007.

Mitchell, D. L., Rasch, P., Ivanova, D., McFarquhar, G., and Nousiaisen, T.: Impact of small ice crystal assumptions on ice sedimentation rates in cirrus clouds and GCM simualtions, Geophys. Res. Lett., 35, L09806, doi:10.1029/2008GL033552, 2008.

Mitchell, D. L., Mishra, S., and Lawson. R. P.: Representing the ice fall speed in climate models: results from Tropical Composition, Cloud and Climate Coupling (TC4) and the Indirect and Semi-Direct Aerosol Campaign (ISDAC), J. Geophys. Res., 116, D00T03, doi:10.1029/2010JD015433, 2011.

Morrison, H. and Gettelman, A.: A new two-moment bulk stratiform cloud microphysics scheme in the Community Atmosphere Model, Version 3 (CAM3). Part I: Description and numerical tests, J. Climate, 21, 3642–3659, doi:10.1175/2008JCLI2105.1, 2008.

Morrison, H. and Grabowski, W. W.: A novel approach for representing ice microphysics in models: description and tests using a kinematic framework, J. Atmos. Sci., 65, 1528–1548, 2008.

Neale, R. B., Chen, C.-C., Gettelman, A., Lauritzen, P. H., Park, S., Williamson, D. L., Conley, A. J., Garcia, R., Kinnison, D., Lamarque, J.-F., Marsh, D., Mills, M., Smith, A. K., Tilmes, S., Vitt, F., Cameron-Smith, P., Collins, W. D., Iacono, M. J., Easter, R. C., Ghan, S. J., Liu, X., Rasch, P. J., and Taylor, M. A.: Description of the NCAR Community Atmosphere Model (CAM 5.0), NCAR Tech. Note NCAR/TN-XXX+STR, 282 pp., Natl. Cent. for Atmos. Res, Boulder, Co, 2010.

Posselt, R. and Lohmann, U.: Introduction of prognostic rain in ECHAM5: design and single column model simulations, Atmos. Chem. Phys., 8, 2949–2963, doi:10.5194/acp-8-2949-2008, 2008.

Prenni, A. J., Harrington, J. Y., Tjernström, M., DeMott, P. J., Avramov, A., Long, C. N., Kreidenweis, S. M., Olsson, P. Q., and Verlinde, J.: Can ice nucleating aerosols affect Arctic seasonal climate?, B. Am. Meteorol. Soc., 88, 541–550, doi:10.1175/BAMS-88-4-541, 2007.

Rasch, P. J. and Kristjansson, J. E.: A comparison of the CCM3 model climate using diagnosed and predicted condensate parameterizations, J. Climate, 11, 1587–1614, 1998.

Rotstayn, L. D.: A physically based scheme for the treatment of stratiform clouds and precipitation in large-scale models. I: Description and evaluation of the microphysical processes, Q. J. Roy. Meteor. Soc., 123, 1227–1282, 1997.

Rotstayn, L. D., Ryan, B. F., and Katzfey, J. J.: A scheme for calculation of the liquid fraction in mixed-phase stratiform clouds in large-scale models, Mon. Weather Rev., 128, 1070–1088, 2000.

Stephens, G. L.: Cloud feedbacks in the climate system: a critical review, J. Climate, 18, 1149–1152, 2005.

Strapp, J. W., Albers, F., Reuter, A., Korolev, A. V., Maixner, U., Rashke, E., and Vukovic, Z.: Laboratory measurements of the response of a PMS OAP-2DC, J. Atmos. Ocean. Tech., 18, 1150–1170, 2001.

Toon, O. B., Starr, D. O., Jensen, E. J., Newman, P. A., Platnick, S., Schoeberl, M. R., Wennberg, P. O., Wofsy, S. C., Kurylo, M. J., Maring, H., Jucks, K. W., Craig, M. S., Vasques, M. F., Pfister, L., Rosenlof, K. H., Selkirk, H. B., Colarco, P. R., Kawa, S. R., Mace, G. G., Minnis, P., and Pickering, K. E.: Planning, implementation, and first results of the Tropical Composition, Cloud and Climate Coupling Experiment (TC4), J. Geophys. Res., 115, D00J04, doi:10.1029/2009JD013073, 2010.

Zhang, K., Liu, X., Wang, M., Comstock, J. M., Mitchell, D. L., Mishra, S., and Mace, G. G.: Evaluating and constraining ice cloud parameterizations in CAM5 using aircraft measurements

from the SPARTICUS campaign, Atmos. Chem. Phys., 13, 4963–4982, doi:10.5194/acp-13-4963-2013, 2013.

Zhao, C., Liu, X., Qian, Y., Yoon, J., Hou, Z., Lin, G., McFarlane, S., Wang, H., Yang, B., Ma, P.-L., Yan, H., and Bao, J.: A sensitivity study of radiative fluxes at the top of atmosphere to cloud-microphysics and aerosol parameters in the community atmosphere model CAM5, Atmos. Chem. Phys., 13, 10969–10987, doi:10.5194/acp-13-10969-2013, 2013.

Comparison of ice particle characteristics

T. Eidhammer et al.

Title Page

Abstract	Introduction
Conclusions	References
Tables	Figures

|◀ | ▶|

◀ | ▶

Back | Close

Full Screen / Esc

Printer-friendly Version

Interactive Discussion
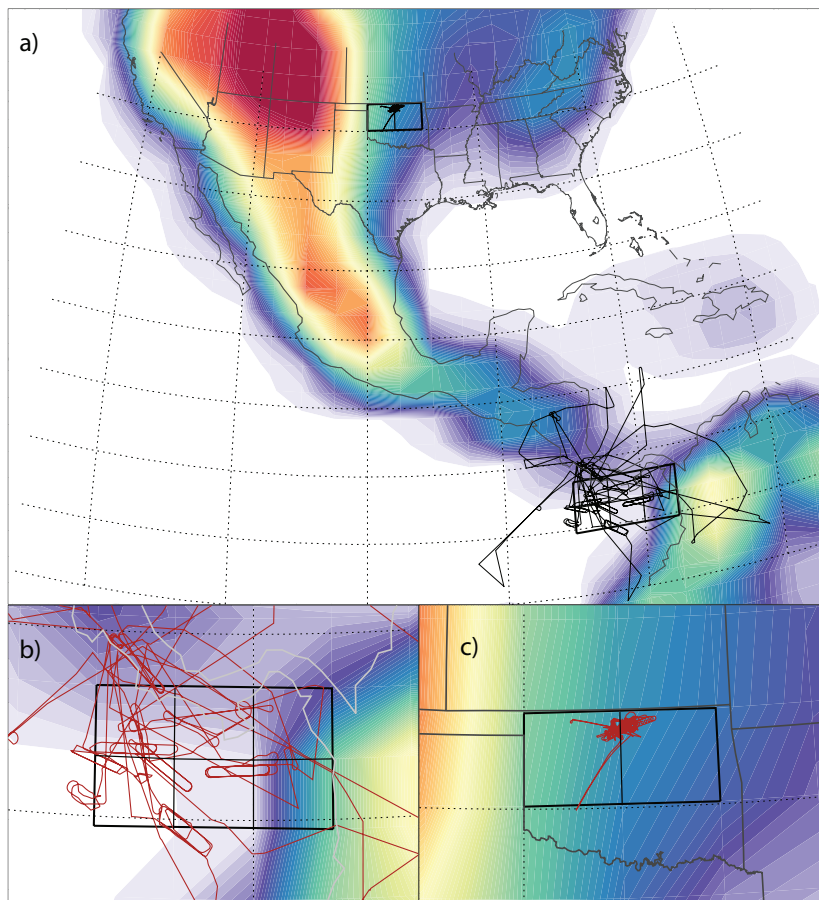
Fig. 1. (a) Location of ARM-IOP and TC4, along with model grid boxes. **(b)** TC4 with a more detailed view of the flight tracks. **(c)** Same as in **(b)** but for ARM-IOP.

Title Page

Abstract   Introduction

Conclusions   References

Tables   Figures

◄   ►►

◄   ►

Back   Close

Full Screen / Esc

Printer-friendly Version

Interactive Discussion
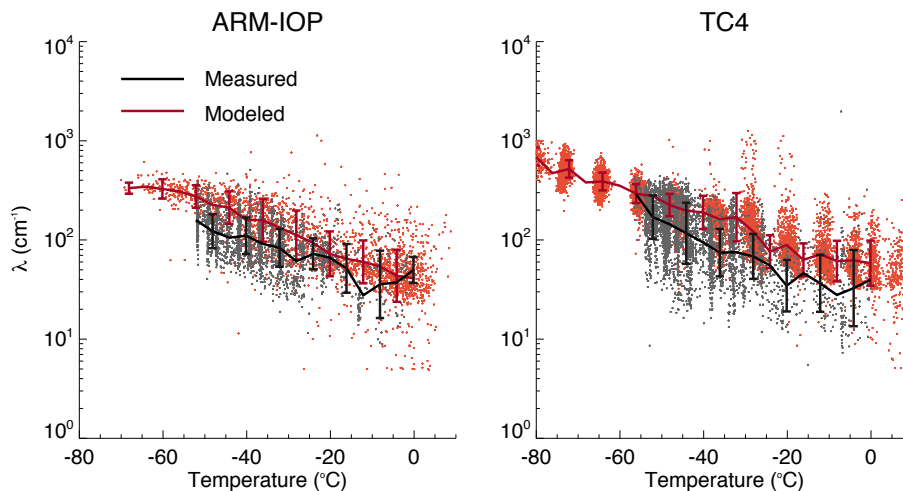
Fig. 2. Slope parameter, modeled (red) and measured (black) for ARM-IOP and TC4. The lines are the geometric mean, the dots represents a fraction of the measurements and modeled values, while the vertical bars represents the geometric standard deviation.
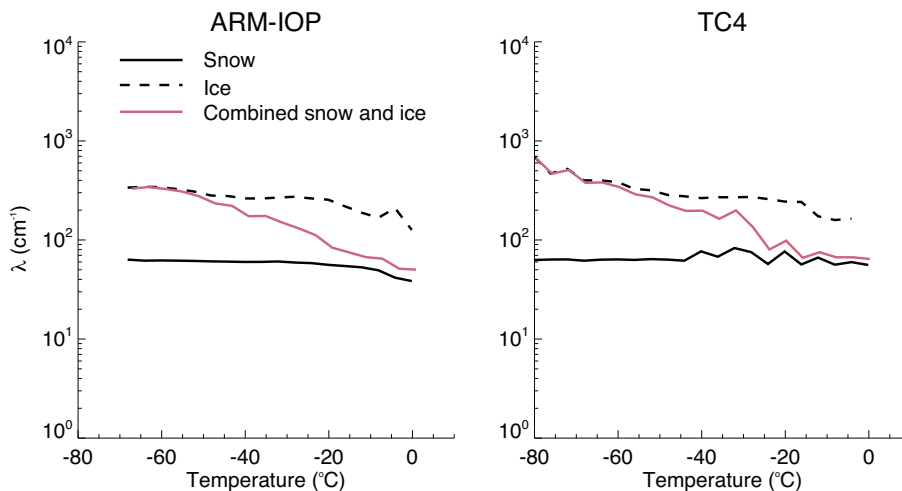
Fig. 3. Modeled slope parameter, for ice and snow individually. Also shown is the combined snow and ice slope parameter, as shown in Fig. 2.

Title Page

Abstract | Introduction

Conclusions | References

Tables | Figures

|◄ | ►|

◄ | ►

Back | Close

Full Screen / Esc

Printer-friendly Version

Interactive Discussion
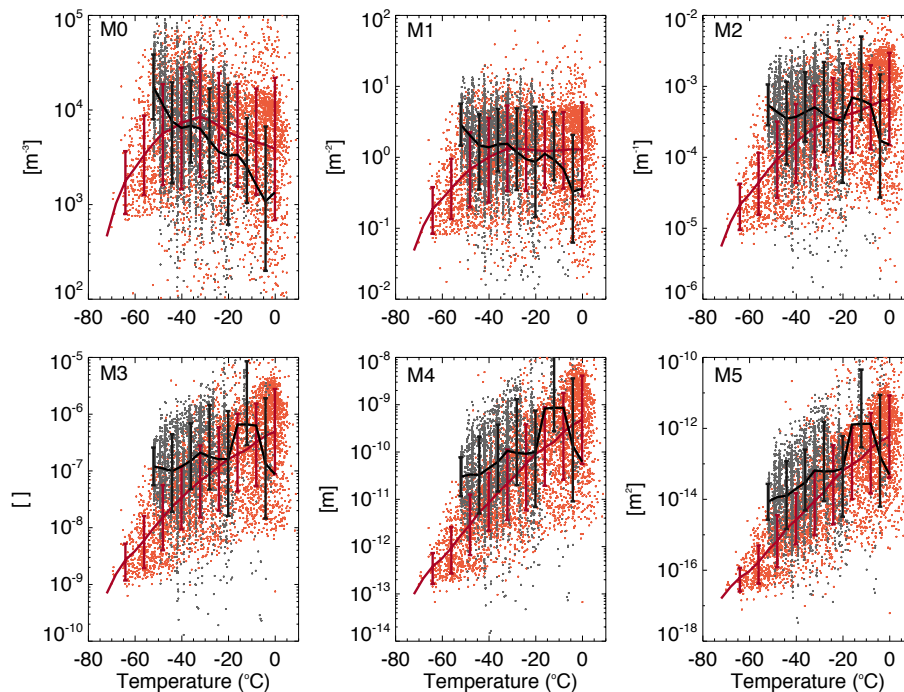
Fig. 4. Moments from ARM–IOP (black: measurements; red: model). Lines are geometric mean, dots represents a fraction of the measurements and model results, while vertical lines are the geometric standard deviation.
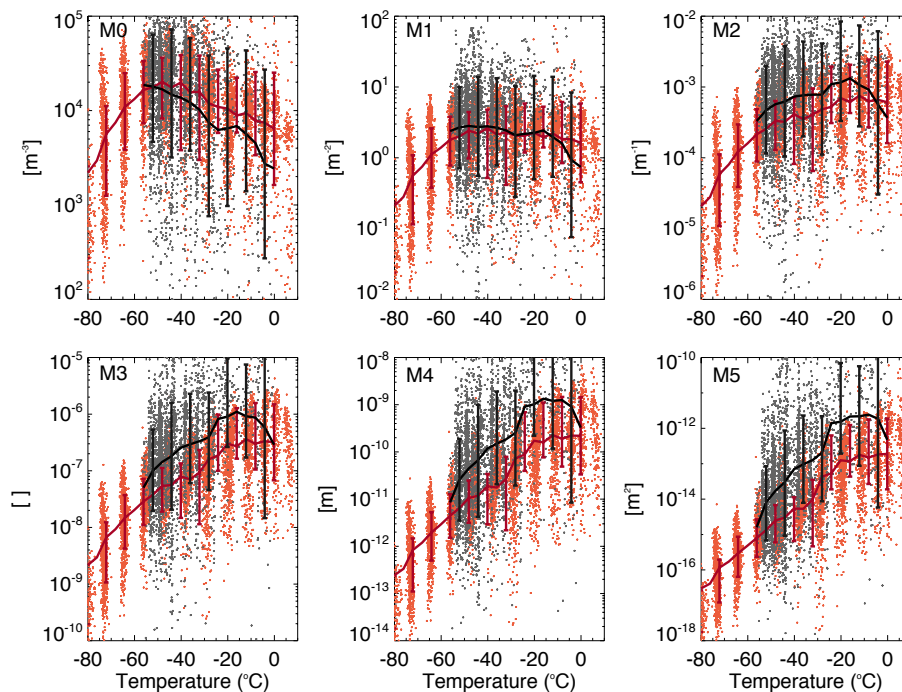
Fig. 5. Same as Fig. 4, but for TC4.
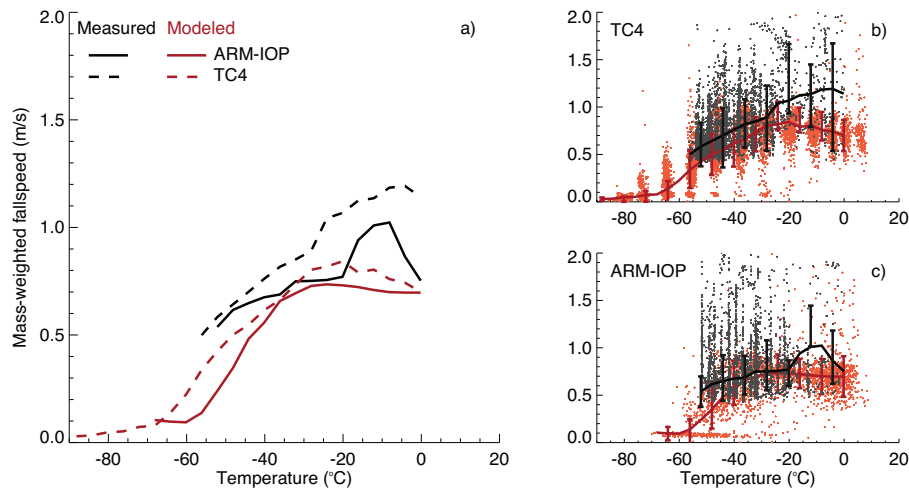
Fig. 6. Mass weighted terminal fall speed. **(a)** Measured and modeled V_m for ARM-IOP and TC4 for comparing fallspeeds between campaigns. (**b** and **c**) Mass weighted fall speeds for showing the measurement and modeling spread.
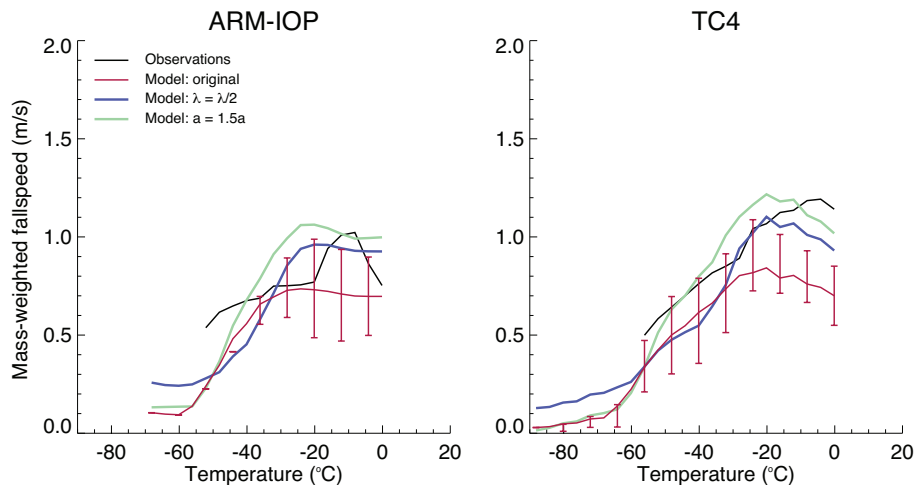
Fig. 7. Mass weighted terminal fall speed with snow and cloud ice $\lambda = \lambda/2$ (blue), and a_i and a_s increased with 50 % (green).
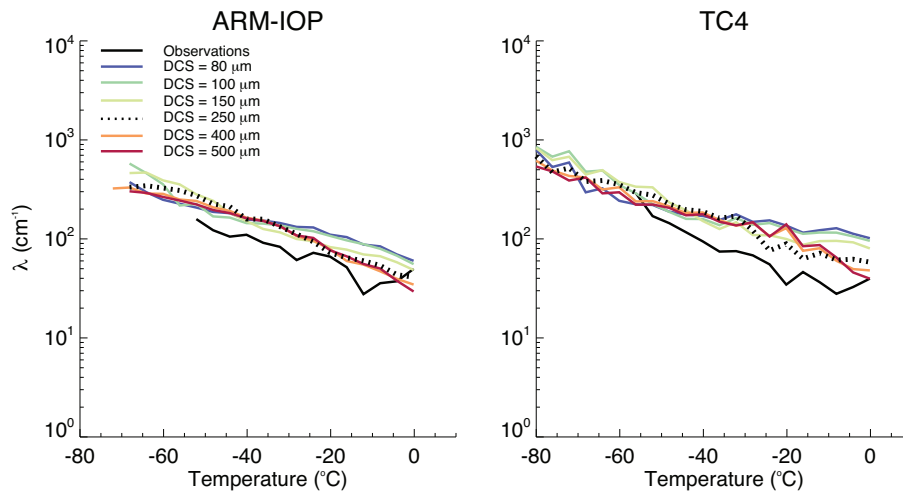
Fig. 8. Same as Fig. 2, but with simulations using different D_{cs} values.
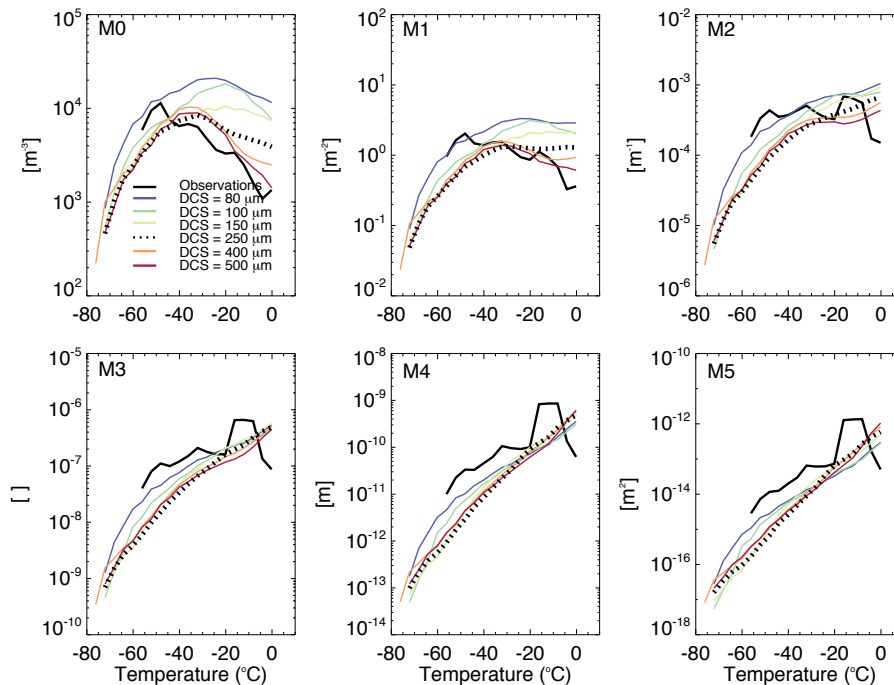
Fig. 9. Same as Fig. 4 (ARM-IOP), but with various D_{cs} values.
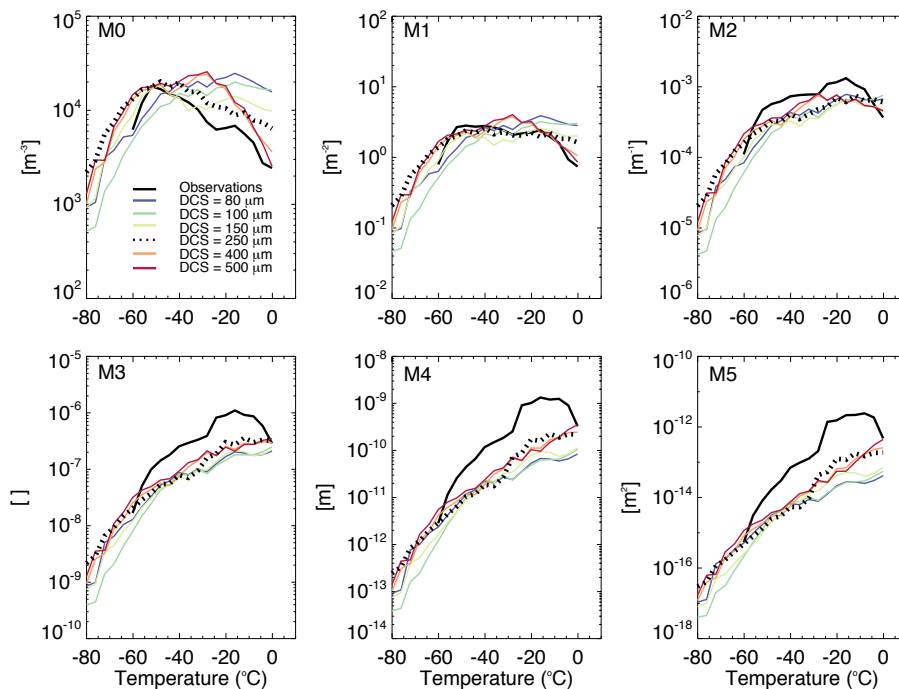
Fig. 10. Same as Fig. 5, (TC4) but with various Dcs values.
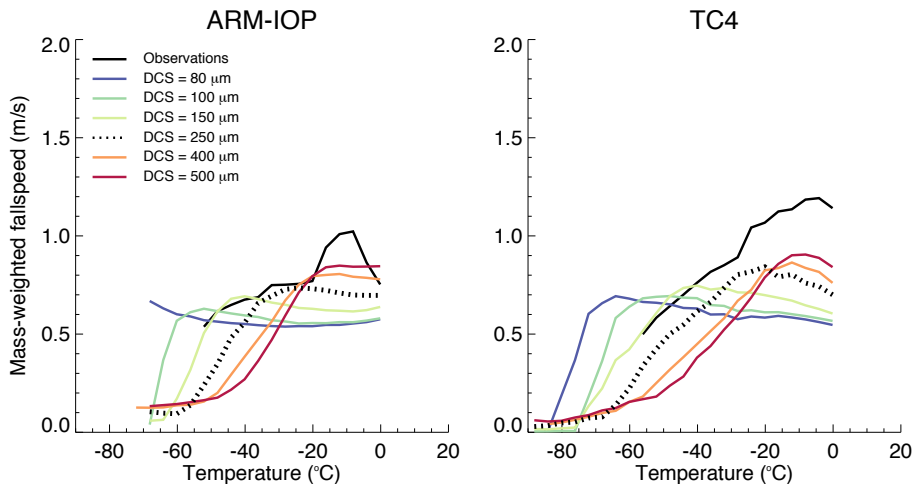
Fig. 11. Same as Figs. 6 and 7, but using different D_{cs} values.
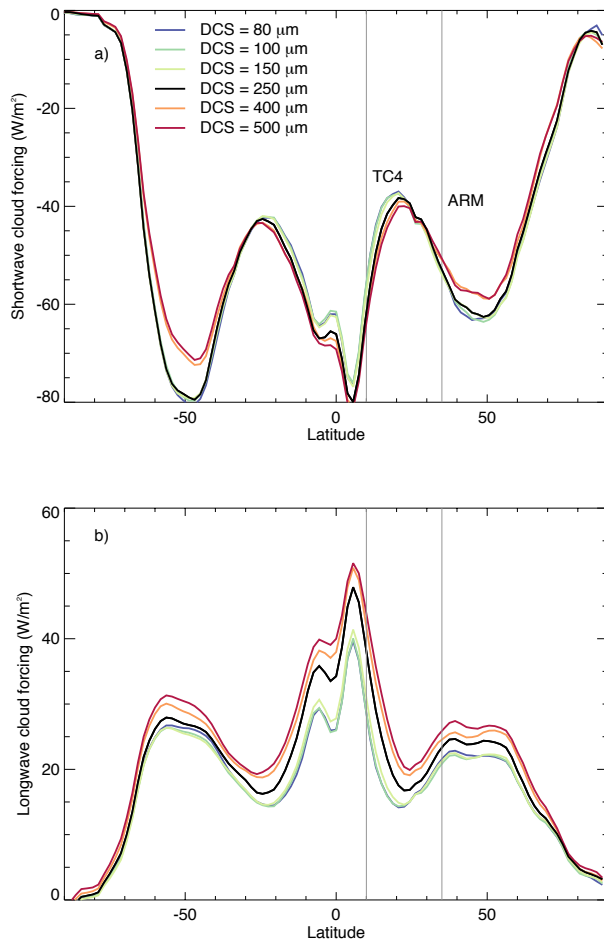
Fig. 12. Zonal averaged shortwave and longwave radiative cloud forcing for the six runs, varying D_{cs}.

Title Page

Abstract | Introduction

Conclusions | References

Tables | Figures

|◄ | ►|

◄ | ►

Back | Close

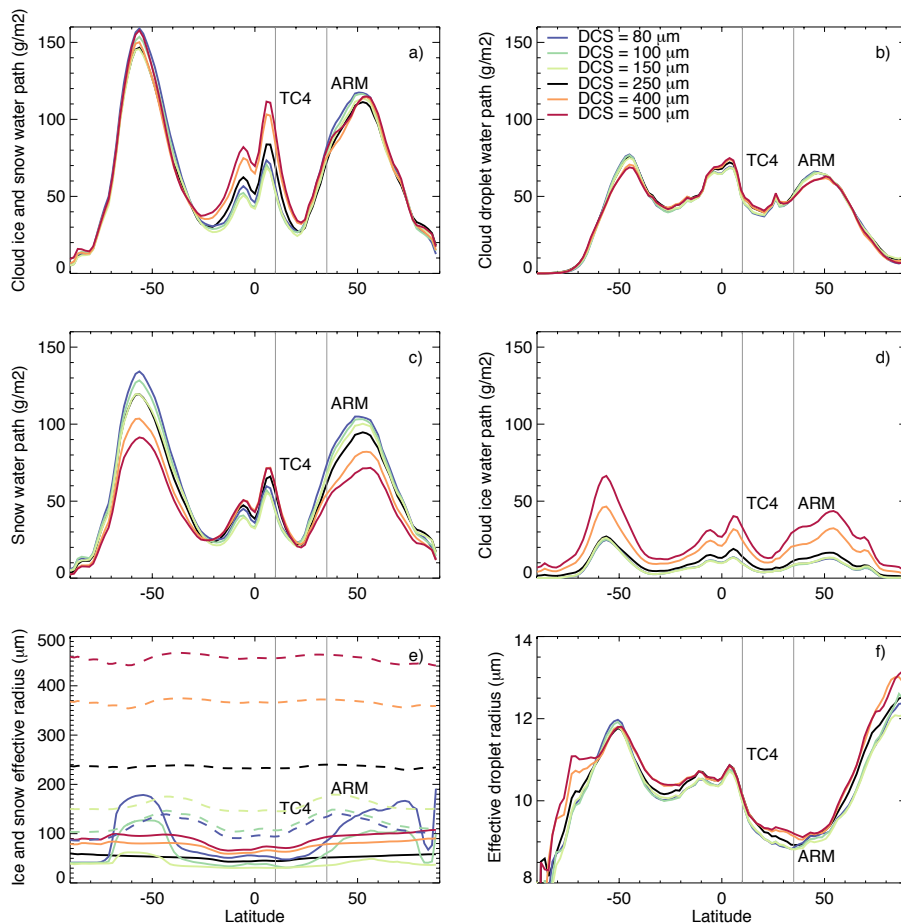Full Screen / Esc

Printer-friendly Version

Interactive Discussion

Fig. 13. Zonal averaged cloud ice and snow water path **(a)**, cloud droplet water path **(b)**, snow water path **(c)**, cloud ice water path **(d)**, ice (solid) and snow (dashed) effective radius **(e)** and effective droplet radius **(d)** for the six different D_{cs} simulations.

Title Page

Abstract | Introduction

Conclusions | References

Tables | Figures

|◄ | ►|

◄ | ►

Back | Close

Full Screen / Esc

Printer-friendly Version

Interactive Discussion
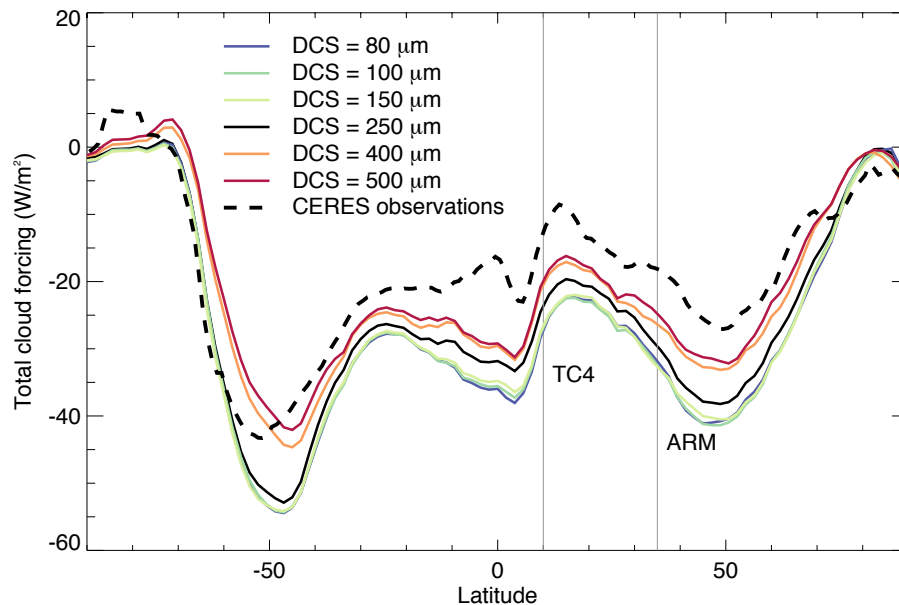
Fig. 14. Total radiative cloud forcing (LWCF + SWCF). Dashed line is observed cloud radiative forcing from CERES.